

## Supporting Information

### **Tumor Microenvironment (TME)-Modulating Nanoreactor for Multiply Enhanced Chemodynamic Therapy Synergized with Chemotherapy, Starvation, and Photothermal Therapy**

*Siyuan Hao<sup>1</sup>, Jingjie Zuo<sup>1</sup>, Haowu Huang<sup>1</sup>, Wenqiu Li<sup>1</sup>, Huiling Guo<sup>1\*</sup>, Mingxing Liu<sup>1</sup>,  
Hongda Zhu<sup>1</sup>, Hongmei Sun<sup>1</sup>*

<sup>1</sup> Key Laboratory of Fermentation Engineering (Ministry of Education), Key Laboratory of Industrial Microbiology in Hubei, National “111” Center for Cellular Regulation and Molecular Pharmaceutics, Cooperative Innovation Center of Industrial Fermentation (Ministry of Education & Hubei Province), School of Bioengineering and Food, Hubei University of Technology, Wuhan 430068, China

\*Corresponding author: [guoguo0302@126.com](mailto:guoguo0302@126.com)

# Contents

<b>Materials and reagents</b> .....	<b>3</b>
<b>Characterization</b> .....	<b>3</b>
<b>Cell Culture</b> .....	<b>4</b>
<b>Animal and tumor models</b> .....	<b>4</b>
<b>Zeta potential</b> .....	<b>5</b>
<b>UV - Visible absorption spectra</b> .....	<b>5</b>
<b>Investigation of stability</b> .....	<b>6</b>
<b>Standard curves of DOX and GOx</b> .....	<b>6</b>
<b>The hydrodynamic size changes of FDPGH</b> .....	<b>7</b>
<b>Schematic illustration of cascade catalysis</b> .....	<b>7</b>
<b>Standard curves and consumption of glucose</b> .....	<b>8</b>
<b>•OH generation and GSH depletion</b> .....	<b>8</b>
<b>The percentage of cell migration area</b> .....	<b>9</b>
<b>Digital photos of 4T1 tumor-bearing mice</b> .....	<b>9</b>
<b>Tumor weights</b> .....	<b>10</b>

## Materials and reagents

Ferrous sulfate heptahydrate ( $\text{FeSO}_4 \cdot 7\text{H}_2\text{O}$ ), ferrous chloride hexahydrate ( $\text{FeCl}_3 \cdot 6\text{H}_2\text{O}$ ), ammonia ( $\text{NH}_3 \cdot \text{H}_2\text{O}$ ), citric acid monohydrate, tris(hydroxymethyl) aminomethane (99%) were purchased from Sinopharm Group Chemical Reagent Co., Ltd. Glucose oxidase (GOx) was purchased from yuanye Bio-Technology Co., Ltd (Shanghai). Dopamine hydrochloride (98%, AR), titanium sulfate ( $\text{Ti}(\text{SO}_4)_2$ ), methylene blue (MB), 5,5'-Dithiobis (2-nitrobenzoic acid) (DTNB) were purchased from Macklin (Shanghai). Doxorubicin (DOX), acridine orange (AO) and thiazolyl blue tetrazolium bromide (MTT) were purchased from Sigma-Aldrich (St. Louis, MO, USA). Hyaluronic acid (HA), hyaluronidase (HAase), bicinchoninic acid (BCA) assay kit, 2',7'-dichlorofluorescein diacetate (DCFH-DA), fluorescein diacetate (FDA), propidium iodide (PI), 5,5',6,6'-Tetrachloro-1,1',3,3'-tetraethyl-imidacarbocyanine iodide (JC-1) kit, Annexin V-fluoresceine isothiocyanate/propidium iodide (Annexin V-FITC/PI) apoptosis and necrosis detection kit were purchased from Beyotime Biotechnology. Bisbenzimidazole H33342 trihydrochloride (Hoechst 33342) was purchased from Solarbio Life Science. Dulbecco's modified Eagle's medium (DMEM), Fetal bovine serum (FBS), antibiotics, trypsin and all other cell culture-related supplies were obtained from Gibco (Carlsbad, CA, USA). All chemicals and solvents were used without further purification. Deionized water was used for all experiments.

## Characterization

Transmission electron microscopy (TEM) and elemental mapping of samples were carried out on a JEM-2100F at 200 kV. Scanning electron microscopy (SEM) images were carried out by a JSM-6480A scanning electron microscopy. The Fourier transform infrared (FTIR) spectrum was detected by an AVATAR 360 FTIR spectrophotometer. The hydrophilic diameter and zeta potential were obtained by using dynamic light scattering (DLS) (Zetasizer Nano, Malvern, UK). X-ray photoelectron spectra (XPS) were acquired on a Thermo Fisher ESCALAB 250 Xi spectrometer using  $\text{Al K}\alpha$  radiation as the excitation source. The UV-vis and fluorescence spectrum were

performed on the UV-1800 spectrophotometer and RF-6000 fluorescence spectrophotometer, respectively. The encapsulation efficacy (EE) and drug loading (DL) of DOX was detected by the ultracentrifugation method. Detailly, the solutions were centrifuged at 10000 rpm for 10 min, collecting all the supernatant and determining via fluorescence spectrophotometer ( $\lambda=480$  nm). Meanwhile, the encapsulation efficacy (EE) and drug loading (DL) of GOx was measured by BCA assay kit. Finally, the EE and DL were calculated by using Eq. (1) and Eq. (2) respectively.

$$\text{EE} (\%) = 100 \times \frac{\text{mass of total DOX} - \text{mass of DOX in supernatant}}{\text{mass of total DOX}} \quad (1)$$

$$\text{DL} (\%) = 100 \times \frac{\text{mass of total DOX} - \text{mass of DOX in supernatant}}{\text{mass of total FDPGH}} \quad (2)$$

### Cell Culture

L929 (mouse fibroblasts cells) and 4T1 (mouse breast cancer cells) were cultured in Dulbecco's Modified Eagle's Medium (DMEM) supplemented with 10% fetal bovine serum (FBS) and 1% antibiotics (penicillin-streptomycin,  $10000 \text{ U}\cdot\text{mL}^{-1}$ ) at  $37^\circ\text{C}$  and humidity of 5%  $\text{CO}_2$ . The cell culture medium was replaced by fresh DMEM medium every 2 days.

### Animal and tumor models

Female BALB/c mice (8-9 weeks) were purchased from the Hubei Provincial Center for Disease Control and Prevention (Wuhan, China). The animal study protocol was approved by the Animal Ethics Committee of Hubei University of Technology and China's Laboratory Animal Affairs Regulations. The mice bearing 4T1 subcutaneous tumor models were constructed through hypodermic injection of  $100 \mu\text{L}$  of PBS containing  $1.0 \times 10^6$  cancer cells into the right back leg, and all the in vivo experiments were carried out when the tumor size reached approximately  $100 \text{ mm}^3$ .

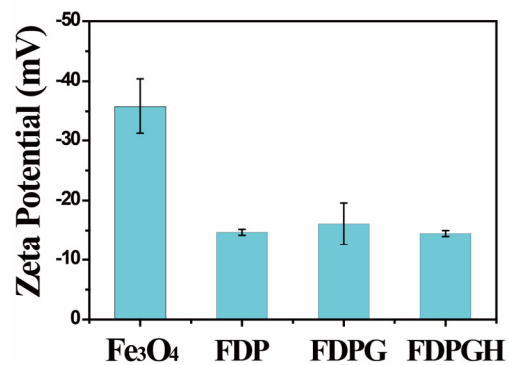


**Figure S1.** Zeta potential of Fe<sub>3</sub>O<sub>4</sub>, FDP, FDPG, FDPGH NPs.

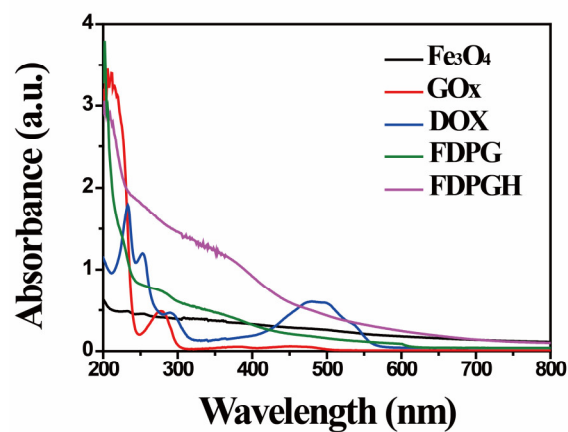


**Fig.S2.** UV-vis of the GOx, Fe<sub>3</sub>O<sub>4</sub>, FDP, DOX, and as-prepared FDPGH nanocomposites.

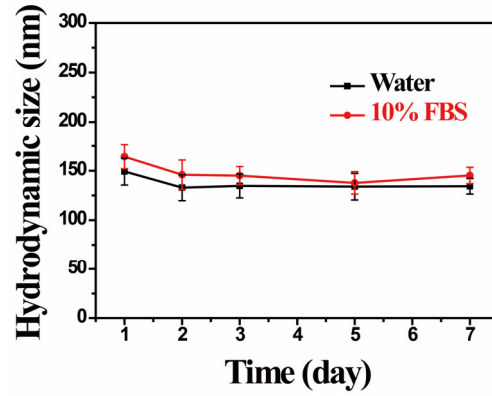


**Figure S3.** Changes in size of FDPGH NPs in water and 10% FBS for 7days (n = 3)

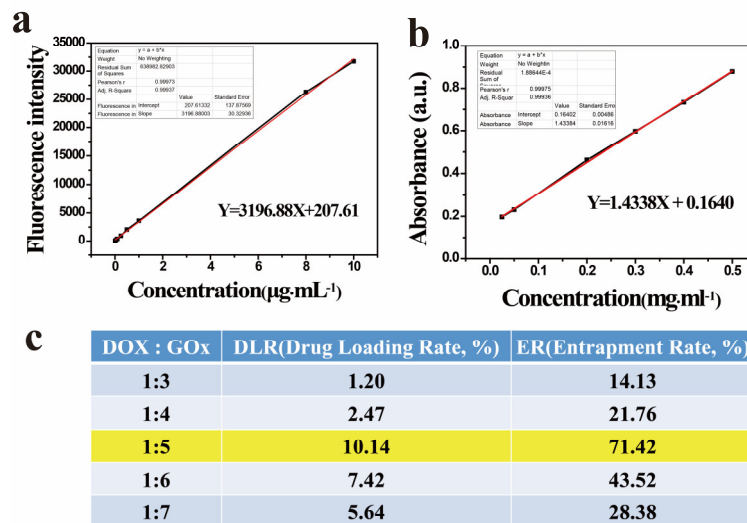


**Figure S4.** Standard curves of absorbance of a) DOX, b) GOx, c) Drug entrapment rate and drug loading capability of nanoparticle under different ratios.

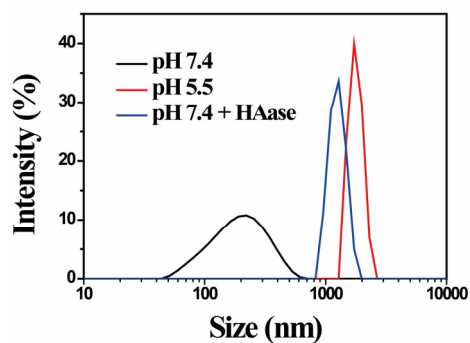


**Figure S5.** The hydrodynamic size changes of FDPGH NPs under different conditions.

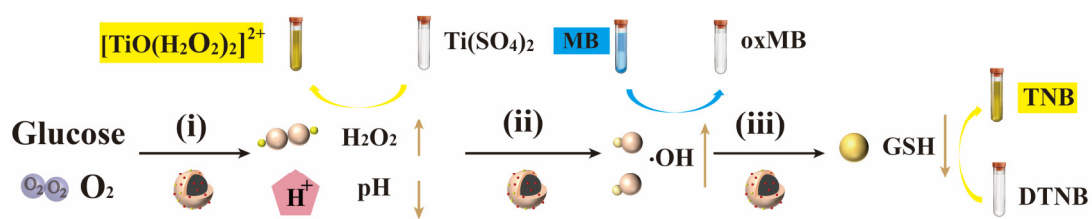


**Figure S6.** Schematic illustration of  $\text{H}_2\text{O}_2$  generation, GSH depletion and  $\cdot\text{OH}$  generation induced by FDPGH NPs.

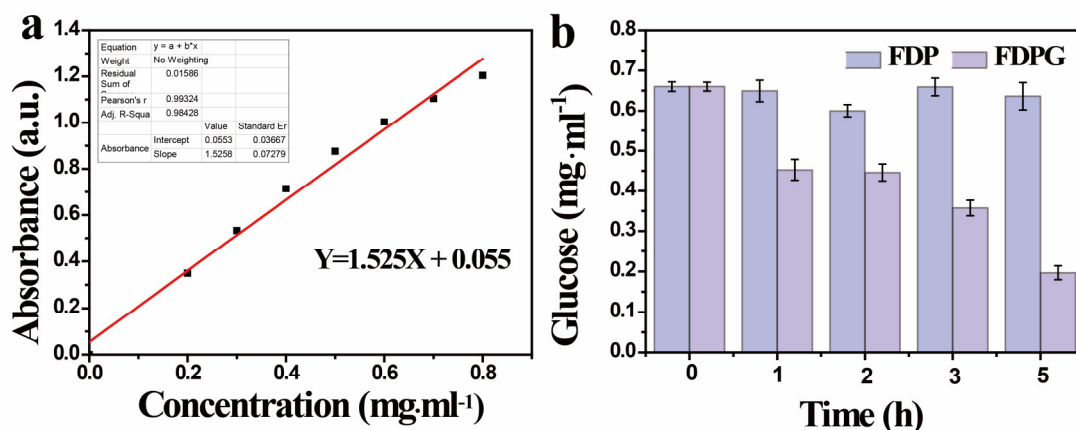


**Figure S7.** a) Standard curves of absorbance of glucose. b) Changes of glucose concentration over time after adding FDP and FDPG.

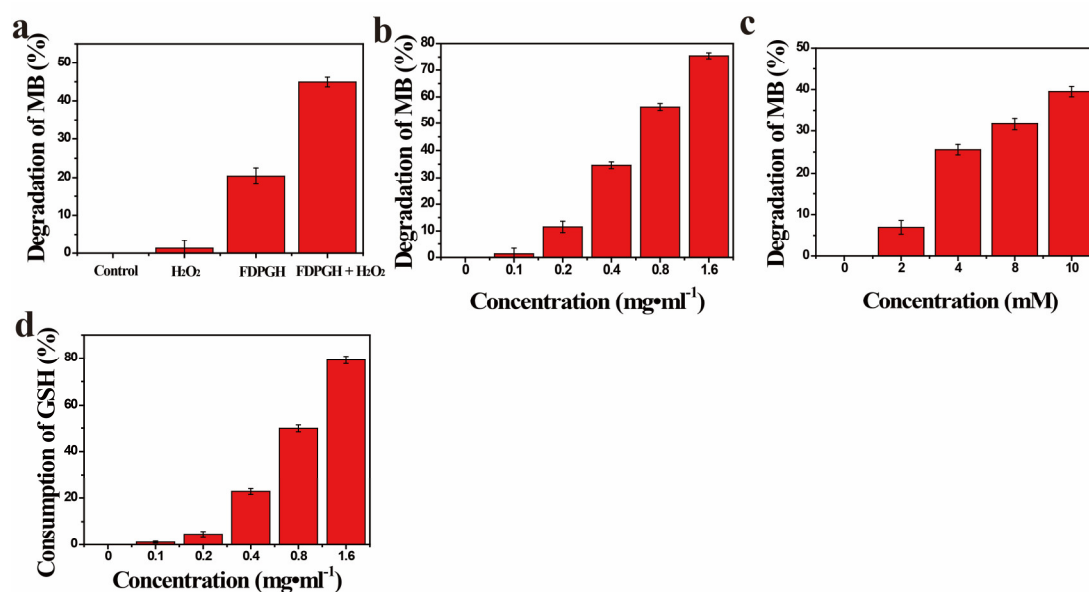


**Figure S8.** MB degradation induced by a) different nanoparticles, varied concentrations of b) FDPGH NPs and c) H<sub>2</sub>O<sub>2</sub>(FDPGH NPs:1.6 mg·ml<sup>-1</sup>). d) GSH depletion by varied concentrations of FDPGH NPs.



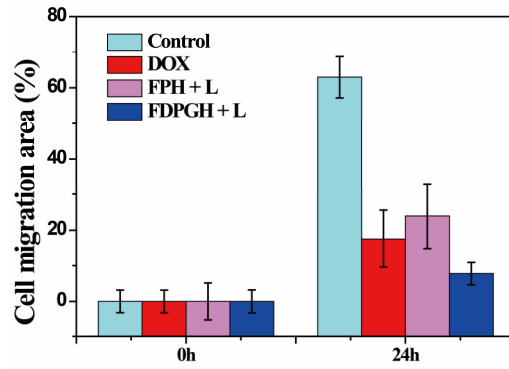


**Figure S9.** Quantification of the percentage of cell migration area after diverse treatments.

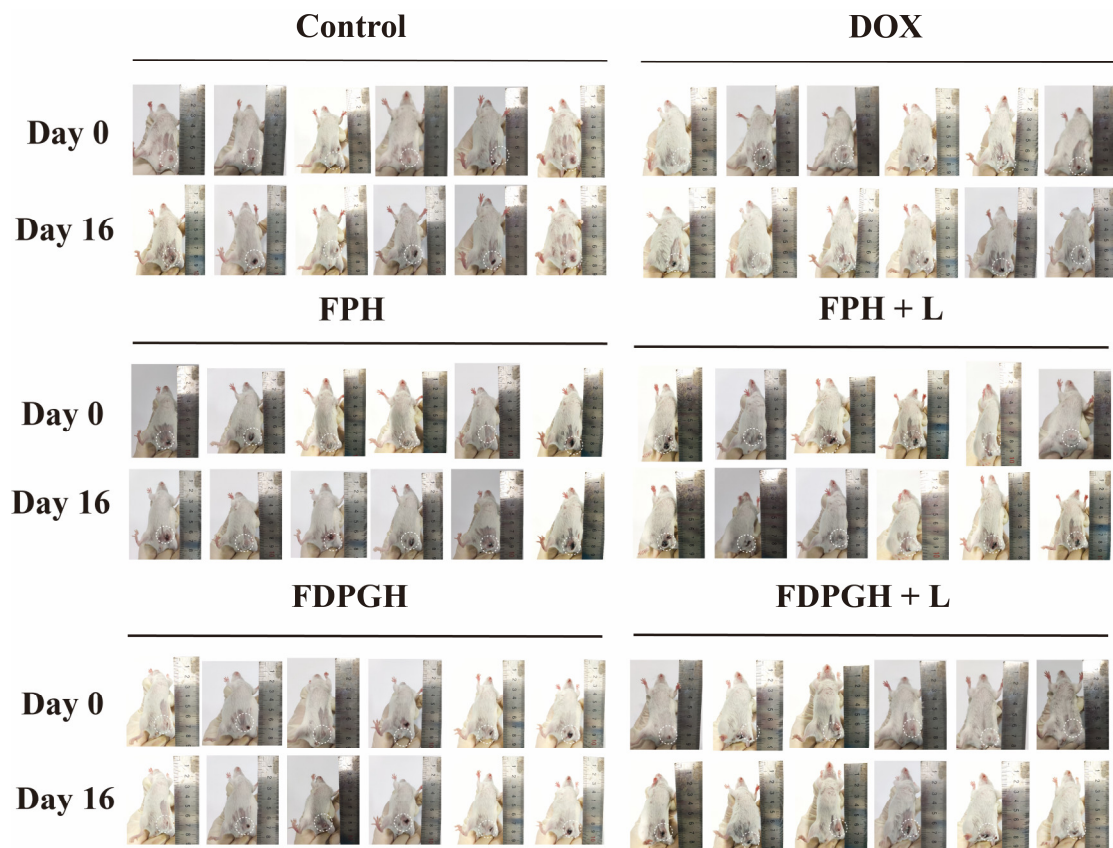


**Figure S10.** Digital photographs of 4T1 tumor-bearing mice after varied treatments at different time intervals (n =6).

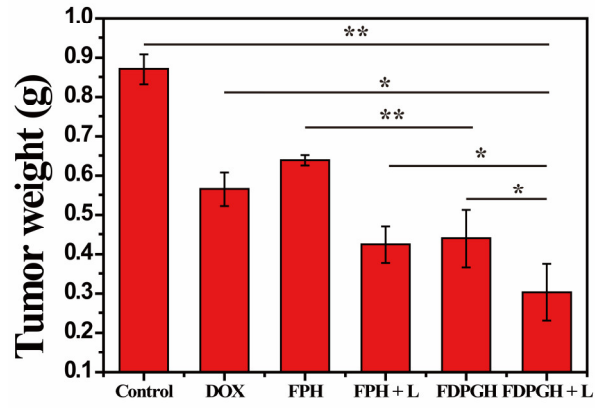


**Figure S11.** The average tumor weights at the endpoint of the indicated treatments. Data are expressed as mean  $\pm$  SD (n = 6). \*  $p < 0.05$ ; \*\*  $p < 0.01$ ; \*\*\*  $p < 0.001$ .